

# Low temperature phase transitions inside CDW phase in kagome metals $AV_3Sb_5$ (A=Cs,Rb,K): Significance of mix-type Fermi surface electron correlations

Huang Jianxin<sup>1</sup>, Rina Tazai<sup>2</sup>, Youichi Yamakawa<sup>1</sup>, Seiichiro Onari<sup>1</sup>, and Hiroshi Kontani<sup>1</sup>

<sup>1</sup>Department of Physics, Nagoya University, Nagoya 464-8602, Japan

<sup>2</sup>Yukawa Institute for Theoretical Physics, Kyoto University, Kyoto 606-8502, Japan

(Dated: June 9, 2023)

To understand the multistage phase transitions in V-based kagome metals inside the charge-density-wave (CDW) phase, we focus on the impact of the “mix-type” Fermi surface because it is intact in the CDW state on the “pure-type” Fermi surface. On the mix-type Fermi surface, moderate spin correlations develop, and we reveal that uniform ( $\mathbf{q} = \mathbf{0}$ ) bond order is caused by the paramagnon interference mechanism, which is described by the Aslamazov-Larkin vertex correction. The most dominant solution is the  $E_{2g}$ -symmetry nematic order, in which the director can be rotated arbitrarily. In addition, we obtain the  $A_{1g}$ -symmetry non-nematic order, which leads to the change in the volume. These results are useful to understand the multistage phase transitions inside the  $2 \times 2$  CDW phase. The present theory has a general significance because mix-type band structure universally exists in various kagome lattice models.

*Introduction.*— Exotic electronic states and correlation-driven superconductivity in kagome metals  $AV_3Sb_5$  (A=K, Cs, and Rb) have attracted increasing attention. Strong Coulomb interaction and the geometrical frustration of V site electrons (in Fig. 1 (a)) give rise to exotic quantum phase transition without magnetization. At ambient pressure ( $P = 0$ ),  $AV_3Sb_5$  exhibits  $2 \times 2$  bond-order (BO) at  $T_{BO} = 78, 94$  and  $102$  K for A=K, Cs and Rb, respectively [1–5]. The BO is the correlation-driven modulation of the hopping integrals ( $\delta t_{ij}$ ) shown in Fig. 1 (b). The superconducting (SC) state appears at  $T_c = 1 \sim 3$  K inside the BO phase [6, 7]. Under pressure,  $T_{BO}$  gradually decreases, while  $T_c$  exhibits non-monotonic pressure dependence [8]. The maximum  $T_c$  ( $\sim 10$  K) is realized around the BO critical pressure  $P_c^{BO} \approx 2$  GPa, consistently with the BO fluctuation pairing mechanism proposed in Ref. [9]. The predicted  $s$ -wave superconductivity has been recently confirmed by the penetration depth and electron irradiation measurements [10, 11].

The nature of rich symmetry-breaking states “inside the BO phase” has been a significant open problem. For example, the  $C_6$  symmetry-breaking nematic state [12, 13] and the time-reversal-symmetry breaking (TRSB) without spin order [4, 14–18] have been reported. These states are caused by the correlation-driven hopping integral modulation:  $\delta t_{ij}$ . The nematic order is given by the bond order with real  $\delta t_{ij}$ , and the TRSB order is given by the imaginary  $\delta t_{ij}$ . The latter accompanies topological charge-current [19] that gives the giant anomalous Hall effect (AHE) [20, 21]. Sizable off-site (beyond-mean-field) interaction [9, 22–40] leads to non-local order parameters ( $\delta t_{ij} \neq 0$ ) in kagome metals.

At present, the onset temperatures of symmetry-breaking states “inside the BO phase” are unsolved. The TRSB order parameter strongly develops below  $T^* = 35 \sim 50$  K in the  $\mu$ -SR [14, 16–18] and the AHE [20, 21] measurements. Notably, the TRSB order is drastically

magnified by the magnetic field  $h$  owing to the  $h$ -bond-current trilinear coupling in the Free energy [35]. As for the nematic state, the scanning birefringence study [13] reports  $T_{nem} \approx T_{BO}$ , while  $T_{nem} \approx 35$  K is reported by the elastoresistance measurement [12]. This discrepancy may indicate that the BO layer stacking with  $\pi$ -shift leads to the weak nematicity at  $T_{BO}$ , and another nematic order emerges inside the BO phase. The origin of the latter nematicity is not understood at present.

In V-based kagome metals, two major Fermi surfaces (FSs) are composed of the  $b_{3g}$ -orbitals and the  $b_{2g}$ -orbitals shown in Fig. 1 (a). The bandstructure and the FSs are shown in Figs. 1 (c) and (d), respectively. Both FSs give large density-of-states (DOS) at the Fermi level due to the van-Hove singularity (vHS) at three M points. The  $b_{3g}$ -orbital FS is called the “pure-FS”, where each vHS point is composed of a single sublattice; see Fig. 1 (e). The vHS points are gapped by the  $2 \times 2$  BO on the pure-FS; see the unfolded FS in Fig. 1 (d). Previous theories have mainly been devoted to understanding the significant roles of the pure-type FS [9, 31–33] except for Refs. [37, 39]. However, one may expect that an additional phase transition below  $T_{BO}$  would occur on the mix-type FS because it is not harmed by the BO. Its sublattice weight is shown in Fig. 1 (f). In addition, it is notable that the mix-type band universally exists in usual kagome lattice models. Therefore, the research on the mix-type band is of great significance.

In this paper, to understand the phase transitions below  $T_{BO}$  in  $AV_3Sb_5$ , we focus on the impact of the mix-type FS because it is intact in the BO phase. On the mix-type FS, moderate spin correlations develop, and it is revealed that the paramagnon interference mechanism leads to the uniform ( $\mathbf{q} = \mathbf{0}$ ) bond order. This beyond-mean-field mechanism is described by the Aslamazov-Larkin vertex correction. The most dominant solution is the  $E_{2g}$ -symmetry nematic order in which the director can be rotated arbitrarily. In addition, we obtain

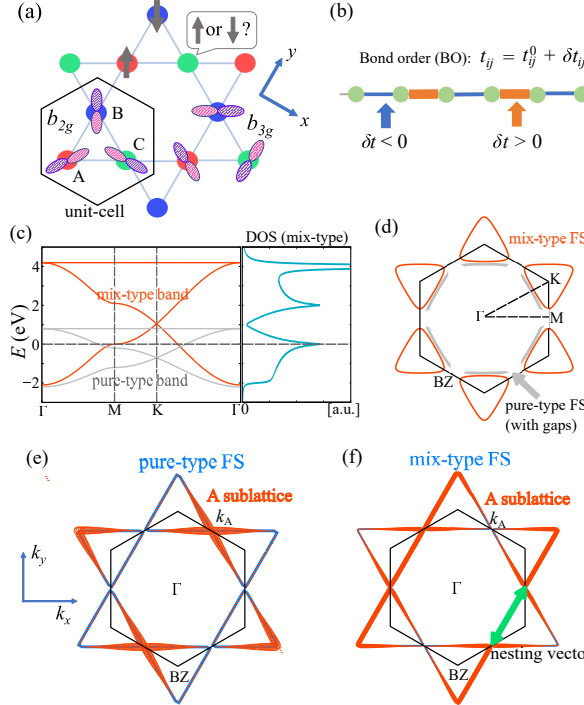


FIG. 1. (a) Kagome lattice structure with geometrical frustration.  $b_{3g}$ - and  $b_{2g}$ -orbitals are shown. (b) BO parameter given by the hopping integral modulation  $\delta t_{ij}$ . (c) Pure-type ( $b_{3g}$ -orbital) and mix-type ( $b_{2g}$ -orbital) band structure with vHS points and the DOS. (d) FSs of pure-type FS ( $n^{\text{pure}} = 2.6$ ) and mix-type FS ( $n^{\text{mix}} = 1.6$ ). Here, the pure-type FS exhibits the  $2 \times 2$  BO induced gap. (e) A-sublattice weight shown by red color on the pure-type FS at the van-Hove filling  $n_{\text{vHF}}^{\text{pure}} = 2.5$ . The vHS point at  $\mathbf{k} = \mathbf{k}_A$  is composed of A sublattice. (f) A-sublattice weight on the mix-type FS at the van-Hove filling  $n_{\text{vHF}}^{\text{mix}} = 1.5$ . The vHS point at  $\mathbf{k} = \mathbf{k}_A$  is composed of B+C sublattices.

the  $A_{1g}$ -symmetry non-nematic order, which leads to the change in the volume. These results are useful to understand the multistage phase transitions inside the  $2 \times 2$  BO phase.

*Model Hamiltonian and Formulations.*— In this paper, we study the quantum phase transition in kagome lattice Hubbard model with a “mix-type” band composed of three  $b_{2g}$  orbitals. We apply the density-wave (DW) equation method to derive the optimized order parameter (= symmetry breaking in the self-energy) driven by the beyond-mean-field vertex corrections. In Ref. [9], the present authors studied the  $b_{2g}+b_{3g}$  orbital kagome lattice Hubbard model for  $\text{AV}_3\text{Sb}_5$ , and found that the pure-type FS alone gives the  $2 \times 2$  BO state. However, the  $b_{2g}$  orbital FS can induce different instabilities for  $T \ll T_{\text{BO}}$ . For this reason, to find the phase transition inside the BO phase, we study the  $b_{2g}$  orbital kagome lattice Hubbard model.

The  $b_{2g}$  orbitals at sublattices A-C are shown in Fig. 1 (a). The corresponding mix-type FS is shown in Fig.

1 (d). The kinetic term of the  $b_{2g}$  orbital model is  $H_0 = \sum_{\mathbf{k},l,m,\sigma} h_{lm}(\mathbf{k}) c_{\mathbf{k},l,\sigma}^\dagger c_{\mathbf{k},m,\sigma}$ , where  $l,m = \text{A}, \text{B}, \text{C}$  and  $\sigma$  is the spin index. In our study the unit of energy (Coulomb interaction, hopping integral and temperature) is eV. We set the nearest-neighbor hopping integral  $t = -0.5$  [9, 31] and put number of electrons on mix-type band  $n^{\text{mix}} = 1.6$ . The  $3 \times 3$  Green function is given as  $\hat{G}(\mathbf{k}, \epsilon_n) = ((i\epsilon_n + \mu)\hat{1} - \hat{h}(\mathbf{k}))^{-1}$ , where  $\epsilon_n = (2n + 1)\pi T$  is the fermion Matsubara frequency.

We also introduce the on-site Coulomb interaction term  $H_U = U \sum_{i,l} n_{i,l,\uparrow} n_{i,l,\downarrow}$ , where  $n_{i,l,\sigma}$  is the electron number at unit cell  $i$ . In the mean-field-level approximation, the spin instability is the most prominent [9]. In the random phase approximation (RPA), spin susceptibility is derived from  $\hat{\chi}^s(\mathbf{q}) = \hat{\chi}^0(\mathbf{q})(\hat{1} - U\hat{\chi}^0(\mathbf{q}))^{-1}$ , where  $\hat{\chi}^0(\mathbf{q})$  is the  $3 \times 3$  irreducible susceptibility matrix and  $\mathbf{q} \equiv (\mathbf{q}, \omega_l = 2\pi Tl)$ . (Note that  $\chi_{l,m}^0(\mathbf{q}) = -T \sum_k G_{l,m}(\mathbf{k} + \mathbf{q})G_{m,l}(\mathbf{k})$ .) The spin susceptibility diverges when the spin Stoner factor  $\alpha_s$ , which is defined as the maximum eigenvalue of  $U\hat{\chi}^0(\mathbf{q})$ , reaches unity. Figure 2 (a) shows the spin susceptibility  $\chi_{\text{A,A}}^s(\mathbf{q})$  at  $T = 0.02$  and  $\alpha_s = 0.97$  ( $U = 2.2$ ). Its maximum peak appears at the nesting of the A-sublattice FS shown in Fig. 1 (f). The real-space short-range spin correlation is depicted in Fig. 2 (b).

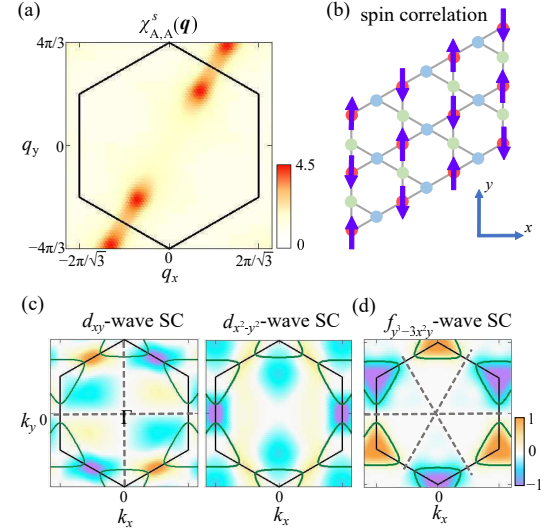


FIG. 2. (a) Spin susceptibility  $\chi_{\text{A,A}}^s(\mathbf{q})$ . Its peak locates on the Brillouin zone. (b) Real-space short-range spin correlation. (c)-(e) SC gap functions given by the gap equation for  $\alpha_s = 0.97$  and  $T = 0.02$ : (c) ( $d_{xy}$ ,  $d_{x^2-y^2}$ )-wave singlet gap with  $\lambda_{\text{SC}} = 0.72$  and (d)  $f$ -wave triplet gap with  $\lambda_{\text{SC}} = 0.44$ .

Here, we shortly discuss the spin-fluctuation-mediated superconductivity on the mix-type FS [31] by solving the linearized gap equation:

$$\lambda_{\text{SC}} \Delta_{lm}(k) = T \sum_{k' l' m'} V_{lm}^{\text{SC}}(k - k') \times G_{ll'}(k') G_{mm'}(-k') \Delta_{l' m'}(k'), \quad (1)$$

where  $V_{lm}^{\text{SC}}(q) = -\frac{3U^2}{2}\chi_{lm}^s(q) + \frac{U^2}{2}\chi_{lm}^c(q) [= \frac{U^2}{2}\chi_{lm}^s(q) + \frac{U^2}{2}\chi_{lm}^c(q)]$  for the spin-singlet [spin-triplet] SC state. Here,  $\lambda_{\text{SC}}$  is the eigenvalue of the gap equation, and  $\Delta_{lm}(k)$  is the gap function. Figures 2 (c)-(d) are the obtained dominant SC gap function for  $\alpha_S = 0.97$  ( $U = 2.2$ ) and  $T = 0.02$ . The obtained largest eigenvalue ( $\lambda_{\text{SC}} = 0.72$ ) corresponds to doubly degenerate  $d_{xy}$ - and  $d_{x^2-y^2}$ -wave singlet state. The  $d_{xy}$ -wave gap function is shown in Fig. 2 (c). In addition, the  $f_{y^3-2x^2y}$ -wave triplet state with  $\lambda_{\text{SC}} = 0.44$  is obtained. This gap function is shown in Fig. 2 (d). Thus, various unconventional pairing states can be realized on the mix-type FS. The  $d$ -wave [ $f$ -wave] SC is caused by the repulsion [attraction] by  $\chi^s(\mathbf{q})$  at  $\mathbf{q} \approx$ nesting vector. Importantly, the  $d$ - and  $f$ -wave SC states would be further stabilized by the nematic-fluctuations on the mix-type FS. In addition, the  $s$ -wave SC state can be mediated by the nematic-fluctuations [9]. This is an important future issue.

*DW equation analysis.*— From now on, we study the phase transition based on the DW equation theory. In this theory, various nonmagnetic DW orders are induced by the beyond-RPA non-local correlations, called the vertex corrections. This theory was first developed to explain the orbital nematic state in Fe-based superconductors, and it has been applied to the cuprates and the twisted-bilayer graphene successfully [29]. Recently, the BO and current order states in kagome metals with pure-type band have been explained [9, 34]. The DW equation for the charge-channel order is given as

$$\lambda_{\mathbf{q}} f_{\mathbf{q}}^L(k) = -\frac{T}{N} \sum_{p, M_1, M_2} I_{\mathbf{q}}^{L, M_1}(k, p) \times \{G(p)G(p + \mathbf{q})\}^{M_1, M_2} f_{\mathbf{q}}^{M_2}(p), \quad (2)$$

where  $I_{\mathbf{q}}^{L, M}(k, p)$  is the “particle-hole (p-h) pairing interaction”,  $k \equiv (\mathbf{k}, \epsilon_n)$  and  $p \equiv (p, \epsilon_m)$  ( $\epsilon_n, \epsilon_m$  are fermion Matsubara frequencies).  $L \equiv (l, l')$  and  $M_i \equiv (m_i, m'_i)$  represent the pair of sublattice indices A, B, C.  $\lambda_{\mathbf{q}}$  is the eigenvalue that represents the instability of the DW at wavevector  $\mathbf{q}$ , and  $\max_{\mathbf{q}}\{\lambda_{\mathbf{q}}\}$  reaches unity at  $T = T_{\text{DW}}$ .  $f_{\mathbf{q}}^L(k)$  is the Hermitian form factor that is proportional to the p-h condensation  $\sum_{\sigma} \{\langle c_{\mathbf{k}+\mathbf{q}, l, \sigma}^{\dagger} c_{\mathbf{k}, l', \sigma} \rangle - \langle \cdots \rangle_0\}$ , or equivalently, the symmetry-breaking component in the self-energy. In real space, the  $\mathbf{k}$ -dependent form factor gives the correlated hopping between  $(i, l)$  and  $(j, m)$ , which is given as:  $\delta t_{il, jm} (= \delta t_{jm, il})^*$ .

$$\delta t_{il, jm} = \frac{1}{N} \sum_{\mathbf{k}} f_{\mathbf{q}}^{lm}(\mathbf{k}) e^{i\mathbf{k} \cdot (\mathbf{r}_{il} - \mathbf{r}_{jm})} e^{i\mathbf{q} \cdot \mathbf{r}_{il}}, \quad (3)$$

where  $\mathbf{r}_{il}$  represents position of  $l$  sublattice in the unit-cell  $i$ . The BO preserves the time-reversal-symmetry:  $\delta t_{il, jm} = \delta t_{jm, il} = \text{real}$ .

The kernel function  $I_{\mathbf{q}}^{L, M}$  in the DW equation is given by the functional derivative of the Luttinger ward function  $\Phi_{\text{LW}}(G)$ . Here, we apply the fluctuation-exchange

approximation for  $\Phi_{\text{LW}}(G)$ . Then,  $I_{\mathbf{q}}^{L, M}$  is composed of one Hartree term, one single-magnon exchange Mak-Thompson (MT) term and two double-magnon interference Aslamazov-Larkin (AL) terms, as depicted in Fig. 3 (a) [29]. Importantly, the AL terms represent the “interference between two paramagnons with momenta  $\mathbf{Q}$  and  $\mathbf{Q}'$ ” that leads to the DW order at  $\mathbf{q} = \mathbf{Q} - \mathbf{Q}'$ ; see Fig. 3 (b).

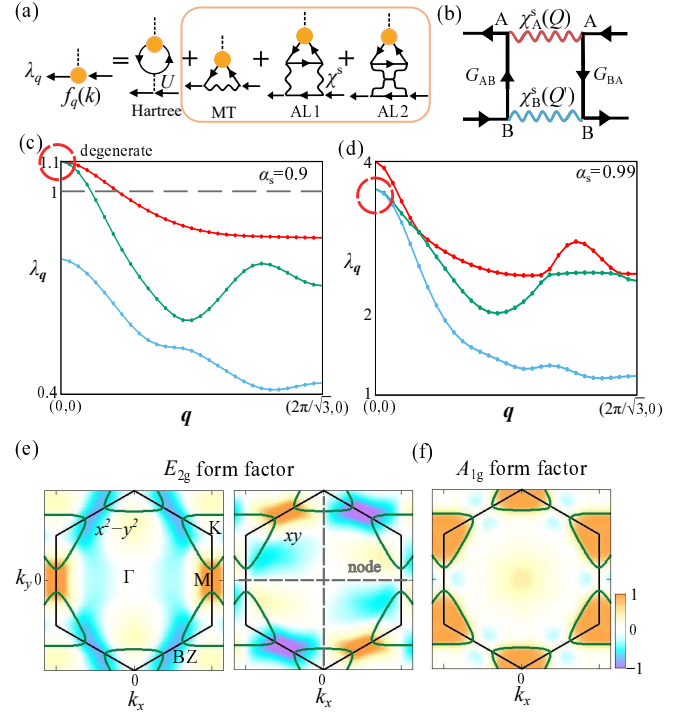


FIG. 3. (a) Linearized DW equation with respect to the form factor  $f_{\mathbf{q}}(k)$  and eigenvalue  $\lambda_{\mathbf{q}}$ . The p-h pairing interaction is composed of the Hartree term, the MT term, and the AL terms. (b) Interference between two paramagnons ( $\mathbf{Q}$  and  $\mathbf{Q}'$ ) that leads to the DW order at  $\mathbf{q} = \mathbf{Q} - \mathbf{Q}'$ . (c-d) Eigenvalue  $\lambda_{\mathbf{q}}$  for two cases: (c) Moderate spin fluctuation case with  $\alpha_S = 0.9$  and (d) strong spin fluctuation case with  $\alpha_S = 0.99$ . The first, second, and third eigenvalues are shown in different colors. In both cases,  $\lambda_{\mathbf{q}}$  exhibits the maximum at  $\mathbf{q} = \mathbf{0}$ . (e-f) Diagonal form factor  $\sum_l f_{\mathbf{q}=0}^{A, B, C}(k)$ : (e)  $E_{2g}$  symmetry solution obtained for  $\alpha_S = 0.9$  and (f)  $A_{1g}$  symmetry solution obtained for  $\alpha_S = 0.99$ . Note that off-diagonal form factor is also large.

With the obtained spin susceptibility, we solve the DW equation. The  $\mathbf{q}$ -dependence of the eigenvalue  $\lambda_{\mathbf{q}}$  at  $n^{\text{mix}} = 1.6$  ( $T = 0.02$ ) is exhibited in Figs. 3 (c) and (d). (Here, we show  $\lambda_{\mathbf{q}}$  only on the path  $\Gamma$ -M because  $\lambda_{\mathbf{q}}$  on the path M-K- $\Gamma$  is small.) Figure 3 (c) [(d)] shows the result for  $\alpha_S = 0.9$  (0.99), where spin fluctuation strength is moderate [strong]. Importantly, the maximum peak position is located at  $\mathbf{q} = \mathbf{0}$  in both cases. The obtained  $\mathbf{q} = \mathbf{0}$  order, which is very different from the nesting driven  $\mathbf{q} \neq \mathbf{0}$  order, is naturally derived from the interference between two paramagnons with wavevectors  $\mathbf{Q}$

and  $\mathbf{Q}'(=\mathbf{Q})$  [29]. For  $\alpha_S = 0.9$  in Fig. 3 (c), the largest eigenvalues are degenerate, and the corresponding form factors are  $E_{2g}$  symmetry BO;  $(\hat{f}_{x^2-y^2}(k), \hat{f}_{xy}(k))$ . The corresponding diagonal form factor  $\sum_l f_{\mathbf{q}=0}^{ll}(k)$  is shown in Fig. 3 (e). Note that off-diagonal form factors are as large as the diagonal form factors. For  $\alpha_S = 0.99$  in Fig. 3 (d), the non-degenerate largest eigenvalue corresponds to  $A_{1g}$  symmetry form factor shown in Fig. 3 (f).

The  $E_{2g}$  symmetry BO gives the nematicity, and its director can be rotated at any angle by taking the linear combination of  $\hat{f}_{x^2-y^2}(k)$  and  $\hat{f}_{xy}(k)$  [24]. To understand the nature of the  $E_{2g}$  symmetry nematic state, we discuss the real-space form factor  $\delta t_{il,jm}$  based on Eq. (3). When the wavevector is  $\mathbf{q} = \mathbf{0}$ ,  $\delta t_{il,jm}$  is simply written as  $\delta t_{lm}(\mathbf{r})$  with  $\mathbf{r} \equiv \mathbf{r}_{il} - \mathbf{r}_{jm}$ . The obtained  $\delta t_{lm}(\mathbf{r})$  for  $f_{x^2-y^2}^{lm}(k)$  at  $\mathbf{q} = \mathbf{0}$  is shown in Fig. 4 (a). (Its schematic picture is given in Fig. 4 (b).) It is plotted in two directions (AB and AC) from sublattice A, as a function of the distance  $R$ , where the distance between nearest sites is 1. The BO along BC direction is the same as that along AC direction. (The even-parity relation  $\delta t_{lm}(R) = \delta t_{ml}(-R)$  is verified.)  $\delta t_{ll}$  at  $R = 0$  represents the onsite charge modulation at sublattice  $l$ , and  $\delta t_{lm}$  at  $R = \pm 1$  ( $l \neq m$ ) represents BO between the nearest sites.

A schematic picture of the hopping modulation due to the nearest BO is given in Fig. 4 (c). In this case, the lattice structure will become nematic in the presence of finite electron-phonon coupling due to  $E_{2g}$  acoustic mode. We also discuss the FS deformation due to the  $E_{2g}$  nematic BO, under the order parameter  $H' = \Delta E \sum_{\mathbf{k}\sigma} \hat{c}_{\mathbf{k}\sigma}^\dagger \hat{f}_\theta(\mathbf{k}) \hat{c}_{\mathbf{k}\sigma}$ , where  $\hat{f}_\theta(\mathbf{k}) \equiv \cos \theta \hat{f}_{x^2-y^2}(\mathbf{k}) + \sin \theta \hat{f}_{xy}(\mathbf{k})$ . The ordered nematic FS at  $\theta = 0$  with  $\Delta E = 0.01$  is showed in Fig. 4 (d). By changing the angle  $\theta$ , the nematic FS can be rotated to any direction. However, the continuous degeneracy with respect to  $\theta$  will be lifted by the 6th order Ginzburg-Landau free energy terms.

Figure 4 (e) shows the  $T$ -dependence of  $\lambda$  for  $E_{2g}$  and  $A_{1g}$  states, in the case of  $U = 1.95$ . The obtained  $\lambda$  monotonically increases with decreasing  $T$ , while the increment of  $\alpha_S$  is moderate (see Fig. 4 (f)). Although the obtained transition temperature is relatively high, it will be reduced to below  $T_{\text{BO}}$  by introducing the self-energy effect [42].

In the SM A [41], we discuss the important roles of the AL and MT vertex corrections for the nematic order. We find that the largest eigenvalue state changes from  $E_{2g}$  BO to  $A_{1g}$  BO at  $\alpha_S \sim 0.975$ . (Simple charge order is prohibited by the Hartree term.) For both even-parity BOs, the AL term gives large positive contribution. In fact, the AL term can stabilize general even-parity BOs, whose wavevector  $\mathbf{q} = \mathbf{Q} - \mathbf{Q}'$  (see Fig. 3 (b)) becomes zero or small (minor) nesting vector [29]. In addition, the MT term slightly favors the nodal  $A_{1g}$  BO. The  $A_{1g}$  BO with  $\lambda_{\mathbf{q}=\mathbf{0}} \sim 1$  will be realized if the self-energy effect

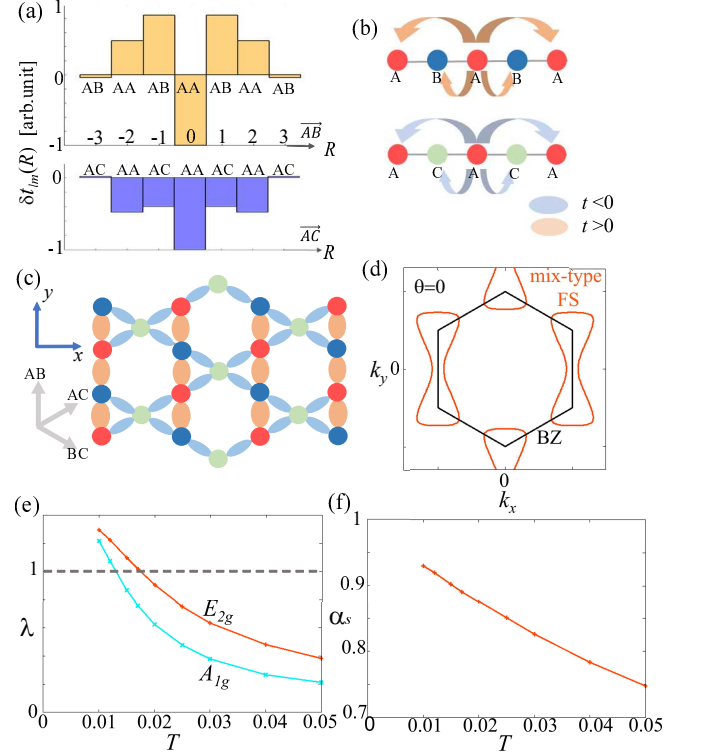


FIG. 4. (a) Real space form factors  $\delta t_{lm}(R)$  in two directions. The horizontal axis means the real space distance. For example, in AB direction,  $R = 1$  (2) marks the hopping modulation between the nearest A and B (A and A). Note that  $\delta t_{AC}(R) = \delta t_{BC}(R)$ . (b) Schematic pictures of  $\delta t_{lm}(R)$ . (c) Nematic bond order in real space for  $\hat{f}_{x^2-y^2}$ . Orange color represents  $\delta t_{ij} > 0$ , while blue color represents  $\delta t_{ij} < 0$ . (d) Nematic FS induced by the nematic BO  $\hat{f}_\theta$ . It can be rotated to any angle by changing the angle  $\theta$ . (e)  $T$ -dependence of  $\lambda_{\mathbf{q}=\mathbf{0}}$  for  $E_{2g}$  and  $A_{1g}$  states, in the case of  $U = 1.95$ . (f)  $T$ -dependence of  $\alpha_S$ .

reduces the eigenvalue by 50% [29].

The quantum interference mechanism produces the nearest site BO in both the mix-type band and the pure-type band models. However, the wavevector is  $\mathbf{q} = \mathbf{0}$  in the mix-type band and  $\mathbf{q} \neq \mathbf{0}$  in the pure-type band. To understand this difference, we focus on the significant role of the vHS points. Since the vHS is composed of two sublattices in the mix-type band, the  $\mathbf{q} = \mathbf{0}$  nearest site BO is efficiently realized by the intra-vHS scattering. In contrast, in the pure-type band, the vHS is composed of a single sublattice, so the inter-site BO should be given by the inter-vHS process at  $\mathbf{q} = \mathbf{q}_{\text{vHS1}} - \mathbf{q}_{\text{vHS2}}$ . Thus, we can understand the different BOs between both bands by using the unique present theory.

*Summary.* — We studied the phase transitions below  $T_{\text{BO}}$  in  $\text{AV}_3\text{Sb}_5$  by focusing on the mix-type FS that is intact in the BO phase. On the mix-type FS, moderate spin correlations develop, and it is revealed that the paramagnon interference mechanism leads to the uniform

( $\mathbf{q} = \mathbf{0}$ ) bond order. The most dominant solution is the  $E_{2g}$ -symmetry nematic order. We also obtain the  $A_{1g}$ -symmetry non-nematic order. These results are useful to understand the multistage phase transitions inside the  $2 \times 2$  BO phase. The present theory has a general significance because mix-type bandstructure exists in many kagome lattice models.

This study has been supported by Grants-in-Aid for Scientific Research from MEXT of Japan (JP18H01175, JP20K03858, JP20K22328, JP22K14003, JP23K03299), and by the Quantum Liquid Crystal No. JP19H05825 KAKENHI on Innovative Areas from JSPS of Japan.

---

[1] B. R. Ortiz, L. C. Gomes, J. R. Morey, M. Winiarski, M. Bordelon, J. S. Mangum, I. W. H. Oswald, J. A. Rodriguez-Rivera, J. R. Neilson, S. D. Wilson, E. Ertekin, T. M. McQueen, and E. S. Toberer, *New kagome prototype materials: discovery of  $KV_3Sb_5$ ,  $RbV_3Sb_5$ , and  $CsV_3Sb_5$* , Phys. Rev. Materials **3**, 094407 (2019).

[2] B. R. Ortiz, S. M. L. Teicher, Y. Hu, J. L. Zuo, P. M. Sarte, E. C. Schueller, A. M. M. Abeykoon, M. J. Krogstad, S. Rosenkranz, R. Osborn, R. Seshadri, L. Balents, J. He, and S. D. Wilson,  $CsV_3Sb_5$ : A  $\mathbb{Z}_2$  Topological Kagome Metal with a Superconducting Ground State, Phys. Rev. Lett. **125**, 247002 (2020).

[3] C. Mu, Q. Yin, Z. Tu, C. Gong, H. Lei, Z. Li, and J. Luo, *S-Wave Superconductivity in Kagome Metal  $CsV_3Sb_5$  Revealed by  $^{121/123}Sb$  NQR and  $^{51}V$  NMR Measurements*, Chin. Phys. Lett. **38**, 077402 (2021).

[4] Y.-X. Jiang, J.-X. Yin, M. M. Denner, N. Shumiya, B. R. Ortiz, G. Xu, Z. Guguchia, J. He, M. S. Hossain, X. Liu, J. Ruff, L. Kautzsch, S. S. Zhang, G. Chang, I. Belopolski, Q. Zhang, T. A. Cochran, D. Multer, M. Litskevich, Z.-J. Cheng, X. P. Yang, Z. Wang, R. Thomale, T. Neupert, S. D. Wilson, and M. Z. Hasan, *Unconventional chiral charge order in kagome superconductor  $KV_3Sb_5$* , Nat. Mater. **20**, 1353–1357 (2021).

[5] H. Li, H. Zhao, B. R. Ortiz, T. Park, M. Ye, L. Balents, Z. Wang, S. D. Wilson, and I. Zeljkovic, *Rotation symmetry breaking in the normal state of a kagome superconductor  $KV_3Sb_5$* , Nat. Phys. **18**, 265–270 (2022).

[6] B. R. Ortiz, P. M. Sarte, E. M. Kenney, M. J. Graf, S. M. L. Teicher, R. Seshadri, and S. D. Wilson, *Superconductivity in the  $\mathbb{Z}_2$  kagome metal  $KV_3Sb_5$* , Phys. Rev. Materials **5**, 034801 (2021).

[7] Q. Yin, Z. Tu, C. Gong, Y. Fu, S. Yan, and H. Lei, *Superconductivity and Normal-State Properties of Kagome Metal  $RbV_3Sb_5$  Single Crystals*, Chin. Phys. Lett. **38**, 037403 (2021).

[8] F. H. Yu, D. H. Ma, W. Z. Zhuo, S. Q. Liu, X. K. Wen, B. Lei, J. J. Ying, and X. H. Chen, *Unusual competition of superconductivity and charge-density-wave state in a compressed topological kagome metal*, Nat. Commun. **12**, 2645 (2021).

[9] R. Tazai, Y. Yamakawa, S. Onari, and H. Kontani, *Mechanism of exotic density-wave and beyond-Migdal unconventional superconductivity in kagome metal  $AV_3Sb_5$  ( $A = K, Rb, Cs$ )*, Sci. Adv. **8**, eabb4108 (2022).

[10] M. Roppongi, K. Ishihara, Y. Tanaka, K. Ogawa, K.

Okada, S. Liu, K. Mukasa, Y. Mizukami, Y. Uwatoko, R. Grasset, M. Konczykowski, B. R. Ortiz, S. D. Wilson, K. Hashimoto, and T. Shibauchi, *Bulk evidence of anisotropic s-wave pairing with no sign change in the kagome superconductor  $CsV_3Sb_5$* , Nat. Commun. **14**, 667 (2023).

[11] W. Zhang, X. Liu, L. Wang, C. W. Tsang, Z. Wang, S. T. Lam, W. Wang, J. Xie, X. Zhou, Y. Zhao, S. Wang, J. Tallon, K. T. Lai, and S. K. Goh, *Nodeless superconductivity in kagome metal  $CsV_3Sb_5$  with and without time reversal symmetry breaking*, Nano Lett. **23**, 872 (2023).

[12] L. Nie, K. Sun, W. Ma, D. Song, L. Zheng, Z. Liang, P. Wu, F. Yu, J. Li, M. Shan, D. Zhao, S. Li, B. Kang, Z. Wu, Y. Zhou, K. Liu, Z. Xiang, J. Ying, Z. Wang, T. Wu, and X. Chen, *Charge-density-wave-driven electronic nematicity in a kagome superconductor*, Nature **604**, 59–64 (2022).

[13] Y. Xu, Z. Ni, Y. Liu, B. R. Ortiz, Q. Deng, S. D. Wilson, B. Yan, L. Balents, and L. Wu, *Three-state nematicity and magneto-optical Kerr effect in the charge density waves in kagome superconductors*, Nat. Phys. **18**, 1470 (2022).

[14] L. Yu, C. Wang, Y. Zhang, M. Sander, S. Ni, Z. Lu, S. Ma, Z. Wang, Z. Zhao, H. Chen, K. Jiang, Y. Zhang, H. Yang, F. Zhou, X. Dong, S. L. Johnson, M. J. Graf, J. Hu, H.-J. Gao, and Z. Zhao, *Evidence of a hidden flux phase in the topological kagome metal  $CsV_3Sb_5$* , arXiv:2107.10714

[15] C. Mielke, D. Das, J.-X. Yin, H. Liu, R. Gupta, Y.-X. Jiang, M. Medarde, X. Wu, H. C. Lei, J. Chang, P. Dai, Q. Si, H. Miao, R. Thomale, T. Neupert, Y. Shi, R. Khasanov, M. Z. Hasan, H. Luetkens, and Z. Guguchia, *Time-reversal symmetry-breaking charge order in a kagome superconductor*, Nature **602**, 245–250 (2022).

[16] R. Khasanov, D. Das, R. Gupta, C. Mielke, M. Elender, Q. Yin, Z. Tu, C. Gong, H. Lei, E. T. Ritz, R. M. Fernandes, T. Birol, Z. Guguchia, and H. Luetkens, *Time-reversal symmetry broken by charge order in  $CsV_3Sb_5$* , Phys. Rev. Research **4**, 023244 (2022).

[17] Z. Guguchia, C. Mielke, D. Das, R. Gupta, J.-X. Yin, H. Liu, Q. Yin, M. H. Christensen, Z. Tu, C. Gong, N. Shumiya, M. S. Hossain, T. Gamsakhurdashvili, M. Elender, P. Dai, A. Amato, Y. Shi, H. C. Lei, R. M. Fernandes, M. Z. Hasan, H. Luetkens, and R. Khasanov, *Tunable unconventional kagome superconductivity in charge ordered  $RbV_3Sb_5$  and  $KV_3Sb_5$* , Nat. Commun. **14**, 153 (2023).

[18] C. Guo, C. Putzke, S. Konyzheva, X. Huang, M. Gutierrez-Amigo, I. Errea, D. Chen, M. G. Vergniory, C. Felser, M. H. Fischer, T. Neupert, and P. J. W. Moll, *Switchable chiral transport in charge-ordered kagome metal  $CsV_3Sb_5$* , Nature **611**, 461–466 (2022).

[19] F. D. M. Haldane, *Model for a Quantum Hall Effect without Landau Levels: Condensed-Matter Realization of the "Parity Anomaly"*, Phys. Rev. Lett. **61**, 2015 (1988).

[20] S.-Y. Yang, Y. Wang, B. R. Ortiz, D. Liu, J. Gayles, E. Derunova, R. Gonzalez-Hernandez, L. Šmejkal, Y. Chen, S. S. P. Parkin, S. D. Wilson, E. S. Toberer, T. McQueen, and M. N. Ali, *Giant, unconventional anomalous Hall effect in the metallic frustrated magnet candidate,  $KV_3Sb_5$* , Sci. Adv. **6**, eabb6003 (2020).

[21] F. H. Yu, T. Wu, Z. Y. Wang, B. Lei, W. Z. Zhuo, J. J. Ying, and X. H. Chen, *Concurrence of anomalous Hall effect and charge density wave in a superconducting topological kagome metal*, Phys. Rev. B **104**, L041103 (2021).

[22] S. Onari and H. Kontani, *Self-consistent Vertex Correction Analysis for Iron-based Superconductors: Mechanism of Coulomb Interaction-Driven Orbital Fluctuations*,

Phys. Rev. Lett. **109**, 137001 (2012).

[23] Y. Yamakawa, S. Onari, and H. Kontani, *Nematicity and Magnetism in FeSe and Other Families of Fe-Based Superconductors*, Phys. Rev. X **6**, 021032 (2016).

[24] S. Onari and H. Kontani, *SU(4) Valley + Spin Fluctuation Interference Mechanism for Nematic Order in Magic-Angle Twisted Bilayer Graphene: The Impact of Vertex Corrections*, Phys. Rev. Lett. **128**, 066401 (2022).

[25] M. Tsuchiizu, Y. Ohno, S. Onari, and H. Kontani, *Orbital Nematic Instability in the Two-Orbital Hubbard Model: Renormalization-Group + Constrained RPA Analysis*, Phys. Rev. Lett. **111**, 057003 (2013).

[26] M. Tsuchiizu, K. Kawaguchi, Y. Yamakawa, and H. Kontani, *Multistage electronic nematic transitions in cuprate superconductors: A functional-renormalization-group analysis*, Phys. Rev. B **97**, 165131 (2018).

[27] A. V. Chubukov, M. Khodas, and R. M. Fernandes, *Magnetism, Superconductivity, and Spontaneous Orbital Order in Iron-Based Superconductors: Which Comes First and Why?*, Phys. Rev. X **6**, 041045 (2016).

[28] R. M. Fernandes, P. P. Orth, and J. Schmalian, *Intertwined Vestigial Order in Quantum Materials: Nematicity and Beyond*, Annu. Rev. Condens. Matter Phys. **10**, 133 (2019).

[29] H. Kontani, R. Tazai, Y. Yamakawa, and S. Onari, *Unconventional density waves and superconductivities in Fe-based superconductors and other strongly correlated electron systems*, Adv. Phys. **70**, 355 (2023).

[30] J. C. S. Davis and D.-H. Lee, *Concepts relating magnetic interactions, intertwined electronic orders, and strongly correlated superconductivity*, Proc. Natl. Acad. Sci. U.S.A. **110**, 17623 (2013).

[31] X. Wu, T. Schwemmer, T. Müller, A. Consiglio, G. Sangiovanni, D. Di Sante, Y. Iqbal, W. Hanke, A. P. Schnyder, M. M. Denner, M. H. Fischer, T. Neupert, and R. Thomale, *Nature of Unconventional Pairing in the Kagome Superconductors  $AV_3Sb_5$  ( $A = K, Rb, Cs$ )*, Phys. Rev. Lett. **127**, 177001 (2021).

[32] M. M. Denner, R. Thomale, and T. Neupert, *Analysis of Charge Order in the Kagome Metal  $AV_3Sb_5$  ( $A = K, Rb, Cs$ )*, Phys. Rev. Lett. **127**, 217601 (2021).

[33] T. Park, M. Ye, and L. Balents, *Electronic instabilities of kagome metals: Saddle points and Landau theory*, Phys. Rev. B **104**, 035142 (2021).

[34] R. Tazai, Y. Yamakawa and H. Kontani, *Charge-loop current order and Z3 nematicity mediated by bond-order fluctuations in kagome metal  $AV_3Sb_5$  ( $A = Cs, Rb, K$ )*, arXiv:2207.08068

[35] R. Tazai, Y. Yamakawa and H. Kontani, *Drastic magnetic-field-induced chiral current order and emergent current-bond-field interplay in kagome metal  $AV_3Sb_5$  ( $A = Cs, Rb, K$ )*, arXiv:2303.00623

[36] T. Schwemmer, H. Hohmann, M. Durrnagel, J. Potten, J. Beyer, S. Rachel, Y.-M. Wu, S. Raghu, T. Müller, W. Hanke, R. Thomale, *Pair Density Wave Instability in the Kagome Hubbard Model*, arXiv:2302.08517

[37] M. H. Christensen, T. Biro, B. M. Andersen, and R. M. Fernandes, *Loop currents in  $AV_3Sb_5$  kagome metals: Multipolar and toroidal magnetic orders*, Phys. Rev. B **106**, 144504 (2022).

[38] F. Grandi, A. Consiglio, M. A. Sentef, R. Thomale, and D. M. Kennes, *Theory of nematic charge orders in kagome metals*, Phys. Rev. B **107**, 155131 (2023).

[39] H. D. Scammell, J. Ingham, T. Li, and O. P. Sushkov, *Chiral excitonic order from twofold van Hove singularities in kagome metals*, Nat. Commun. **14**, 605 (2023).

[40] A. Ptak, A. Kobialka, M. Sternik, J. Lazewski, P.T. Jochym, A.M. Oles, and P. Piekarz, *Dynamical study of the origin of the charge density wave in  $AV_3Sb_5$  ( $A = K, Rb, Cs$ ) compounds*, Phys. Rev. B **105**, 235134 (2022).

[41] Supplementary Materials.

[42] R. Tazai, S. Matsubara, Y. Yamakawa, S. Onari, and H. Kontani, *Rigorous formalism for unconventional symmetry breaking in Fermi liquid theory and its application to nematicity in FeSe*, Phys. Rev. B **107**, 035137 (2023).

## [Supplementary Materials]

Huang, Jianxin<sup>1</sup>, Rina Tazai<sup>2</sup>, Youichi Yamakawa<sup>1</sup>, Seiichiro Onari<sup>1</sup>, and Hiroshi Kontani<sup>1</sup>

<sup>1</sup>Department of Physics, Nagoya University, Nagoya 464-8602, Japan

<sup>2</sup>Yukawa Institute for Theoretical Physics, Kyoto University, Kyoto 606-8502, Japan

### A: Important Roles of the AL and MT Vertex Corrections

Here, we discuss the important roles of the AL and MT vertex corrections for the nematic order. Figure S1 (a) shows the obtained  $\lambda_{\mathbf{q}=0}$  for the  $E_{2g}$  solution and that for the  $A_{1g}$  solution as functions of  $\alpha_s$  for  $T = 0.02$ . These eigenvalues reach unity for  $\alpha_S \sim 0.9$ . With increasing  $\alpha_S$ , the largest eigenvalue state changes from  $E_{2g}$  BO to  $A_{1g}$  BO at  $\alpha_s \sim 0.975$ . (Simple charge order is prohibited by the Hartree term.) Figures S1 (b) and (c) give the eigenvalue contributed from the AL and MT terms for the fixed form factor,  $\lambda_q^{\text{AL}}$  and  $\lambda_q^{\text{MT}}$ , respectively. (Note that  $\lambda_q = \lambda_q^{\text{AL}} + \lambda_q^{\text{MT}}$ .) For both  $E_{2g}$  and  $A_{1g}$  channels, the AL term gives large positive contribution. In fact, the AL term can stabilize general even-parity BOs, whose wavevector  $\mathbf{q} = \mathbf{Q} - \mathbf{Q}'$  (see Fig. 3 (b) in the main text) becomes zero or small (minor) nesting vector [1]. The AL processes give the relation  $\lambda_{E_{2g}}^{\text{AL}} \gtrsim \lambda_{A_{1g}}^{\text{AL}}$ ; see Fig. S1 (b). Thus, the nodal  $A_{1g}$  BO originates from the large MT term; see Fig. S1 (c). The  $A_{1g}$  BO with  $\lambda_{\mathbf{q}=0} \sim 1$  will be realized if the self-energy effect reduces the eigenvalue by 50% [1].

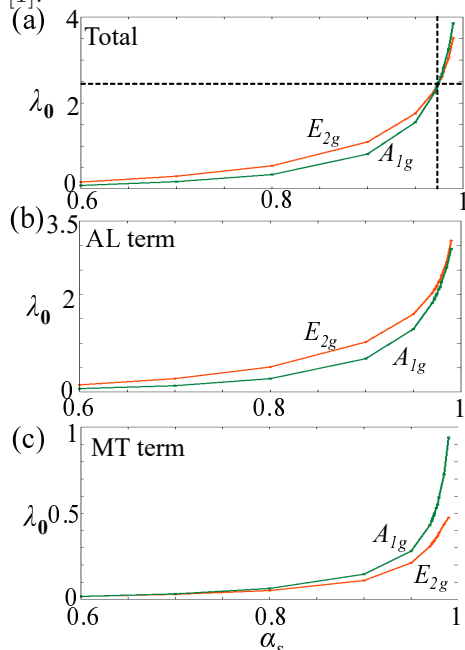


FIG. S1. (a)  $\lambda_{\mathbf{q}=0}$  for the  $E_{2g}$  solution and that for the  $A_{1g}$  solution as functions of  $\alpha_s$  for  $T = 0.02$ . These eigenvalues reach unity for  $\alpha_S \sim 0.9$ . With  $\alpha_s \lesssim 0.975$ , the  $E_{2g}$  solution has the largest  $\lambda$ . For  $\alpha_s \gtrsim 0.975$ , it is replaced with the  $A_{1g}$  solution. (b)(c) Eigenvalue contributed from the AL and MT terms,  $\lambda_q^{\text{AL}}$  and  $\lambda_q^{\text{MT}}$ , respectively. (Note that  $\lambda_q = \lambda_q^{\text{AL}} + \lambda_q^{\text{MT}}$ .) While the AL term gives the dominant contribution to  $\lambda_{\mathbf{q}=0}$ , the MT term plays an important role in determining the symmetry and nodal structure of the form factor.

[1] H. Kontani, R. Tazai, Y. Yamakawa, and S. Onari, *Unconventional density waves and superconductivities in Fe-based superconductors and other strongly correlated electron systems*, Adv. Phys. **70**, 355 (2023).